Seasonal climate summary southern hemisphere (spring 2014): El Niño continues to try to break through, and Australia has its warmest spring on record (again!)

Pandora Hope[1], Phillip Reid[2], Skie Tobin[1], Matthew Tully[1], Andrew Klekociuk[3], Paul Krummel[4]

[1] Bureau of Meteorology, Melbourne, Australia
[2] Bureau of Meteorology, Hobart, Australia
[3.] Australian Antarctic Division, Hobart, Australia
[4.] CSIRO Oceans and Atmosphere, Aspendale, Australia

(Manuscript received November 2015; accepted December 2015)

Southern hemisphere circulation patterns and associated anomalies for the austral spring 2014 are reviewed, with emphasis given to the Pacific Basin climate indicators and Australian rainfall and temperature patterns. Equatorial sea-surface temperatures in the Pacific warmed through the season, and the Southern Oscillation just exceeded El Niño thresholds. However, although trade wind strength weakened at times, particularly late in the season, tropical cloudiness near the Date Line and trade wind strength were more often close to average, suggesting the atmosphere was still not firmly linked with the warmer ocean below. The negative Indian Ocean Dipole values of winter flipped to neutral or weakly positive values through spring. Pressures in the Australian and Maritime Continent regions were high. Around Antarctica, sea ice reached a record extent in September, with expansion most prominent in the Indian Ocean sector and north of the Ross Sea. Winds to the north of these regions were strong. The Antarctic ozone hole was of moderate severity, and of similar size to ozone holes in the early 1990s.

Over Australia, it was the warmest spring on record, surpassing the record warm spring of 2013. A strong anomaly in the 200 hPa geopotential height persisted over the south-east of the country through October and November. Australia was particularly dry in the east through spring, but Western Australia received good rainfall. Column ozone levels in the Australian region were slightly above average and consistent with increased ozone transport to mid-latitudes associated with the phase of the Quasi-Biennial Oscillation.

Introduction

This summary reviews the southern hemisphere and equatorial climate patterns for spring 2014, with particular attention given to the Australasian and Pacific regions. The main sources of information for this report are analyses prepared by the Bureau of Meteorology.

Corresponding author address: Pandora Hope, Bureau of Meteorology, GPO Box 1289, Melbourne VIC 3001, Australia.
Email: p.hope@bom.gov.au

Pacific and Indian Basin climate indices

Southern Oscillation Index

The Troup Southern Oscillation Index[1] (SOI) for the period January 2008 to June 2015 is shown in Figure 1, together with a five-month weighted moving average. Sustained departures of the SOI from neutral values (generally considered to be between +8 and –8) can reflect El Niño–Southern Oscillation (ENSO) events; sustained positive values may indicate La Niña, while sustained negative values may indicate El Niño. The five-month weighted average SOI value approached El Niño thresholds throughout spring 2014 after remaining mostly within the neutral range since February 2012 (the end of the 2011 La Niña). Monthly SOI values for the spring 2014 season were –7.5, –8.0 and –10.0 for September, October and November respectively, averaging to a spring SOI of –8.5. Mean Sea Level Pressure (MSLP) at Darwin was higher than average for all months of spring, with anomalies with respect to 1933–1992 average of +1.1, +0.9 and +1.1 hPa respectively, while MSLP in Tahiti was only slightly below average, with anomalies of –0.2, –0.4 and –0.4 hPa for each month. Although these values suggest El Niño, other atmospheric indicators were not as emphatic.

Figure 1 Southern Oscillation Index, from January 2008 to June 2015, together with a five-month binomially weighted moving average. The means and standard deviations used in the computation of the SOI are based on the period 1933–1992.

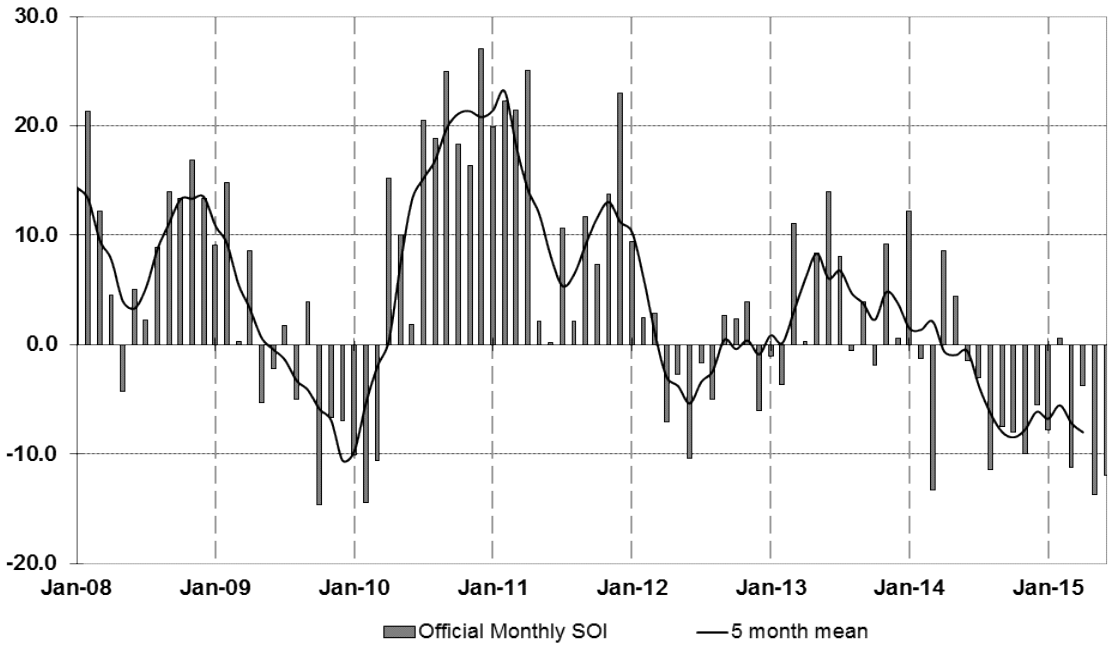

Multivariate ENSO index (MEI)

The Multivariate ENSO Index (MEI), produced by the US Climate Diagnostics Center, is derived from a number of atmospheric and oceanic parameters, which are typically associated with ENSO, and is calculated as a two-month mean. Significant negative values indicate La Niña, while significant positive values indicate El Niño. Monthly values had been neutral since winter 2012 before they started to rise at the beginning of 2014 (Figure 2) and remained around +0.8 during winter, they dropped again into spring. The bi-monthly values for the spring 2014 season were +0.50, +0.36, +0.71, +0.58 for Aug–Sep, Sep–Oct, Oct–Nov and Nov–Dec respectively. These values are less indicative of an El Niño signature than what was suggested by the SOI. The way the MEI is formed means that aspects of the wider spatial variability of the temperature, wind, cloud and pressure are captured by this index, which can provide greater information than can be gleaned

[1] The Troup Southern Oscillation Index (Troup 1965) used in this article is ten times the standardised monthly anomaly of the difference in mean sea level pressure (MSLP) between Tahiti and Darwin. The calculation is based on a sixty-year climatology (1933–1992). The Darwin MSLP is observed at Darwin Airport WMO 94120 and provided by the Bureau of Meteorology. Tahiti MSLP is observed at Papeete Airport WMO 91938 and provided by Météo France inter-regional direction for French Polynesia.

from the SOI alone. Thus, although pressure over Darwin was high, the wider Pacific basin did not reflect a fully developed El Niño.

Figure 2 Bi-monthly Multivariate ENSO Index values from January 2011 to December 2014, together with a weighted average of three bi-monthly values.

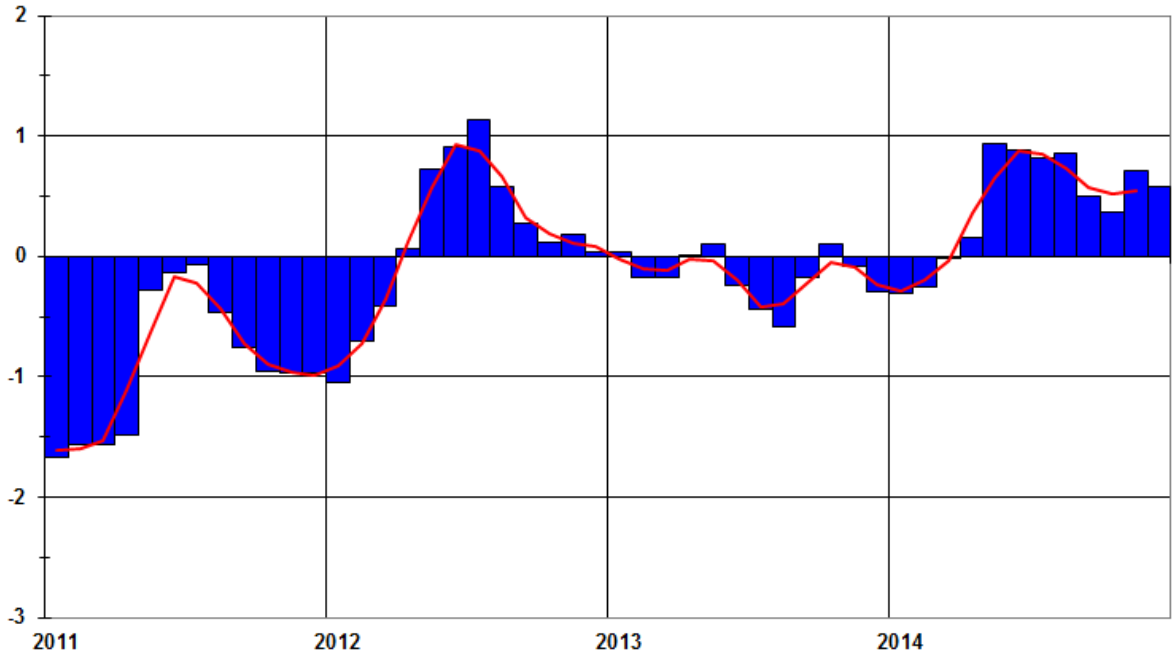

Outgoing long-wave radiation

ENSO can be tracked through changes in the strength and location of anomalous convection over the tropical Pacific, e.g. during El Niño, convection around the Date Line is enhanced. Changes in outgoing long-wave radiation (OLR) over the tropics are due mostly to changes in convection, with increases in OLR associated with decreased convection and reduced cloud cover, while decreases can be associated with increased cloud and convection.

Standardised monthly anomalies of OLR[2] are computed for a tropical region about the Date Line, 5°S to 5°N and 160°E to 160°W, by the Climate Prediction Center at the US National Oceanic and Atmospheric Administration (NOAA). Monthly values for austral spring were +0.2 Wm^{-2}, –0.1 Wm^{-2} and +0.4 Wm^{-2} for September, October and November respectively. Thus, although the SOI was indicative of El Nino conditions, convection was likely suppressed near the Date Line in two months of the austral spring 2014 season, suggesting that the atmosphere was not coupling strongly to the underlying warm oceans.

The spatial pattern of seasonal OLR anomalies across the globe is shown in Figure 3. The OLR pattern in the western Pacific was inconsistent with El Niño, and the mixture of anomalies near the Date Line and the near-average values along the equator in the eastern Pacific were more typical of a neutral ENSO state. The OLR anomalies were positive over the Maritime Continent with a large region of above average OLR (decreased convection) off Sumatra, extending west to around 90°E and north into south-east Asia and south to northern Australia. In the Indian Ocean, a large region of weakly below average OLR (increased convection) is evident in the western north Indian Ocean extending from the equator to the subcontinent. Over the continents there was an extensive band of negative OLR in near tropical northern Africa, through Western Australia, and also in Central America.

[2] Obtained from http://www.cpc.ncep.noaa.gov/data/indices/olr.

Figure 3 OLR anomalies for spring 2014 (W/m2). Base period is 1979–2000.

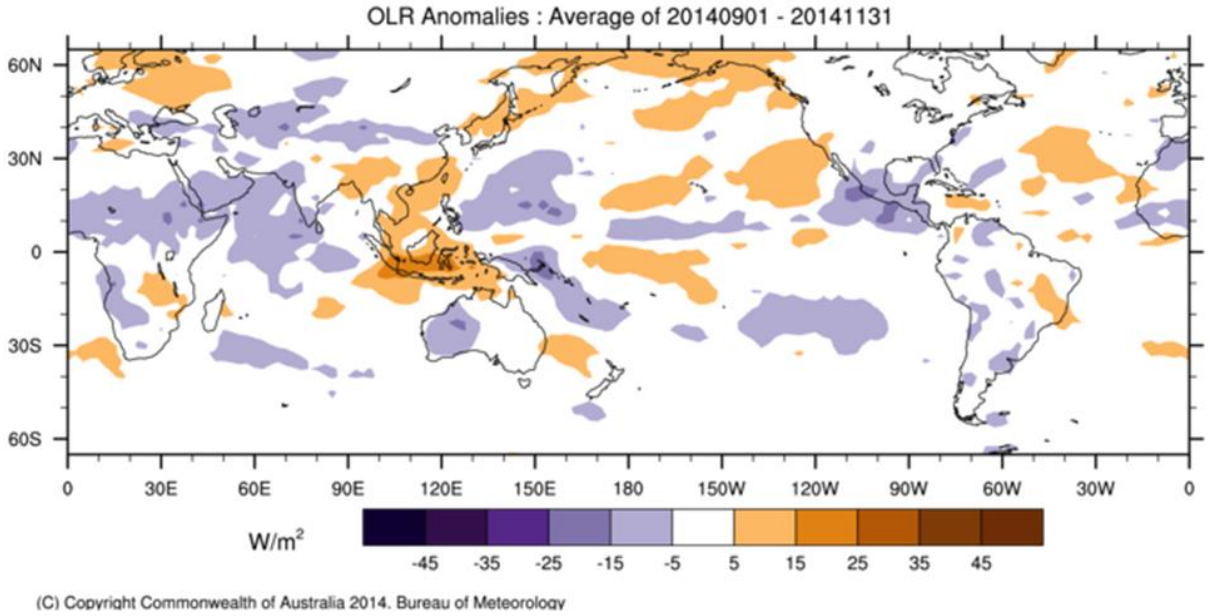

Indian Ocean Dipole (IOD)

A positive IOD is characterised by cooler water around Indonesia in the eastern Indian Ocean and warmer water in the tropical western Indian Ocean. Positive IOD events, often associated with lower rainfall in central and southeastern Australia in spring, are more likely to occur during El Niño. The IOD can be represented by the Dipole Mode Index (DMI), and sustained values of the DMI below –0.4 °C indicate a negative IOD event, while sustained values above +0.4 °C indicate a positive IOD event. The DMI is the difference in SST anomalies between a western node centred on the equator off the coast of Somalia (50°E to 70°E and 10°S to 10°N) and an eastern node in the Southern Hemisphere around Sumatra (90°E to 110°E and 10°S to 0°S). Weekly values of the DMI were lower than –0.4 °C throughout winter, but flipped to weakly positive values early in spring and continued positive throughout the season (Figure 4). During this period only one week's value exceeded +0.4 °C; thus the IOD was considered neutral through spring.

Figure 4 Weekly DMI values from July 2010 to March 2015.

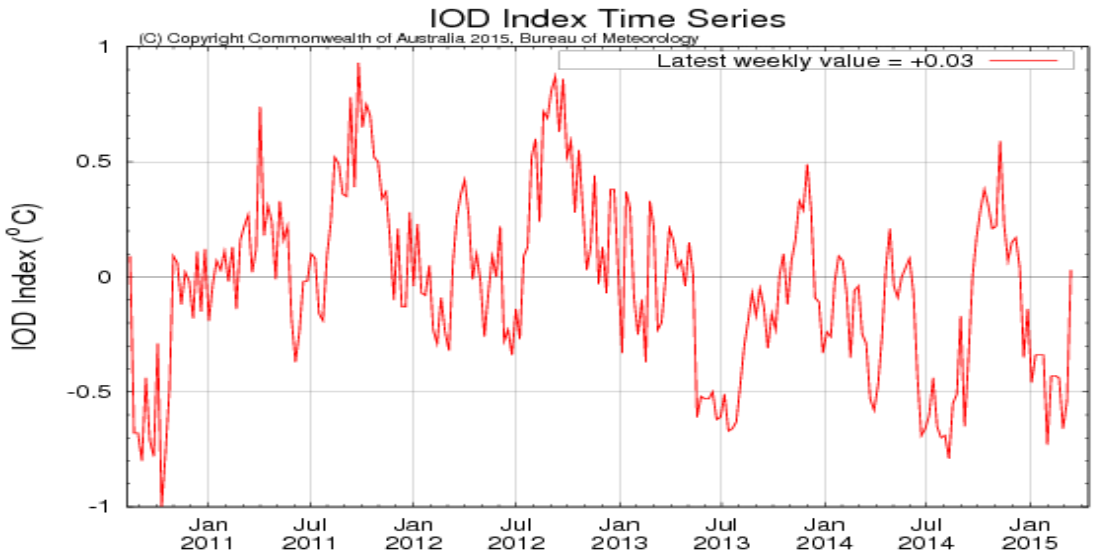

Madden–Julian Oscillation (MJO)

The MJO can be characterised as an eastward moving 'pulse' of cloud and rainfall near the equator that typically recurs every 30 to 60 days. The MJO is monitored by the Real-time Multivariate MJO (RMM) index. A description of this index and the associated phases can be found in Wheeler and Hendon (2004).

There was little MJO activity throughout austral spring (Figure 5) until late in the season when an active pulse of the MJO becomes evident over the Indian Ocean, shifting over the Maritime Continent in the final week, and into the Western Pacific in early December. Impacts from the activity in November would typically result in reduced rainfall over south-east Australia and easterly wind anomalies over eastern Australia.

Figure 5 Phase-space representation of the MJO index for September, October and November 2014. Daily values are shown in red, green and blue for September, October and November respectively.

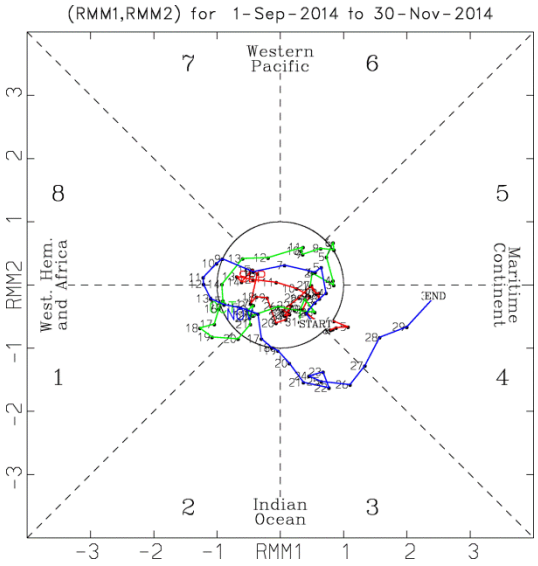

The enhanced convection associated with the MJO event at the end of the season in the Indian Ocean is evident in the time-longitude section plot of OLR anomalies in late November in the left panel of Figure 6. Associated with this are enhanced westerly winds (Figure 6, right panel), with weakened winds further east around the dateline. These anomalies however did not persist. Earlier in the season there were no sustained wind anomalies, which worked to weaken the build-up of an El Niño in 2014.

Oceanic patterns

Sea surface temperatures (SSTs)

Figure 7 shows spring 2014 SST anomalies in degrees Celsius (°C). These have been obtained from the US NOAA Optimum Interpolation analyses (Reynolds et al. 2002). SSTs in the Pacific Ocean were anomalously warm right along the equator and throughout the north Pacific. The entire Indian Ocean was also generally warmer than average. There were cool anomalies in the seas to the north of Australia and off the South American coast. Most anomalies in tropical regions were small and the SST pattern for austral spring 2014 does not look like a typical El Niño pattern. As northern continents moved into their autumn, anomalies in the northern reaches of each ocean basin were warm, with some small cool regions, likely due to circulation anomalies (see section below). There were generally cool anomalies around Antarctica. Antarctic sea ice reached record extent in 2014 (see section on sea ice below). Table 1 shows that the NINO anomalies were all positive for all months of austral spring, however, monthly values of NINO3.4 reached the El Niño threshold of +0.8 °C for

only one month, in November. The threshold, however, failed to be sustained from the second half of December and into the new year.

Figure 6 Time-longitude section of daily-averaged OLR and 850 hPa westerly wind anomalies, averaged for 15°S to 15°N, for the period July 2014 to December 2014. Anomalies are with respect to a base period of 1979–2010.

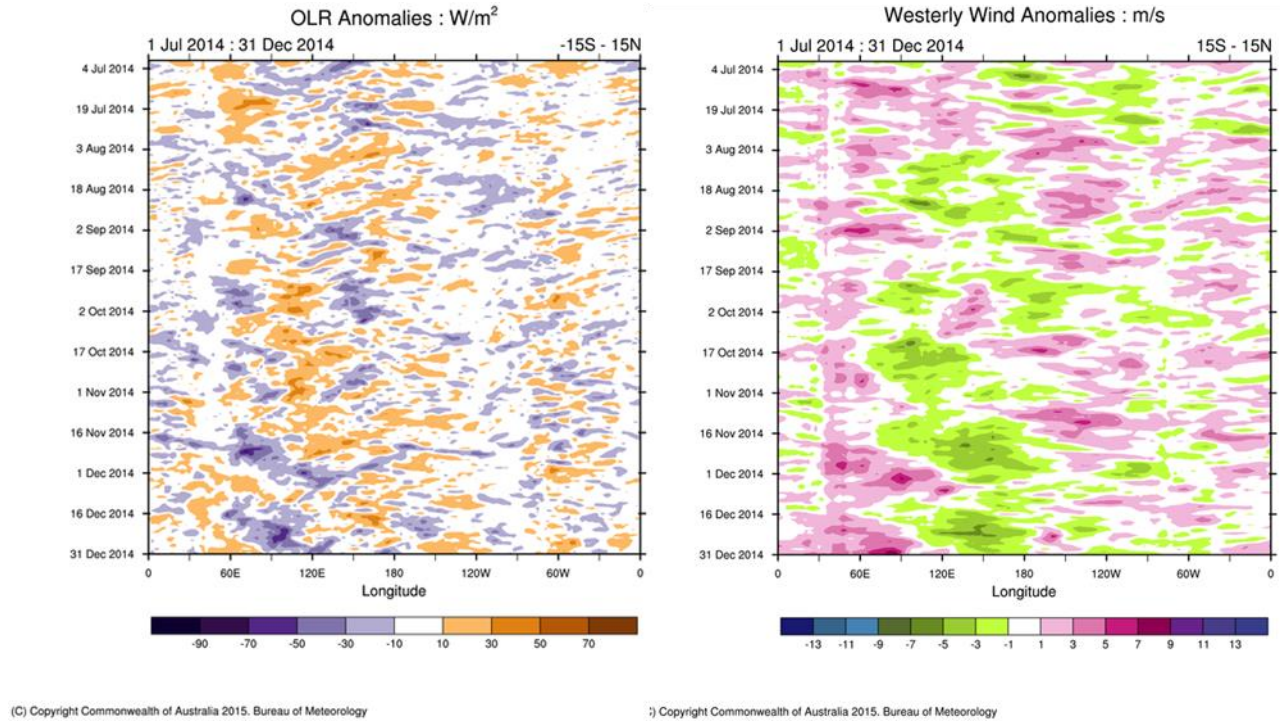

Figure 7 Anomalies of SST for spring 2014 (°C), calculated against a 30-year climatology (1961–1990).

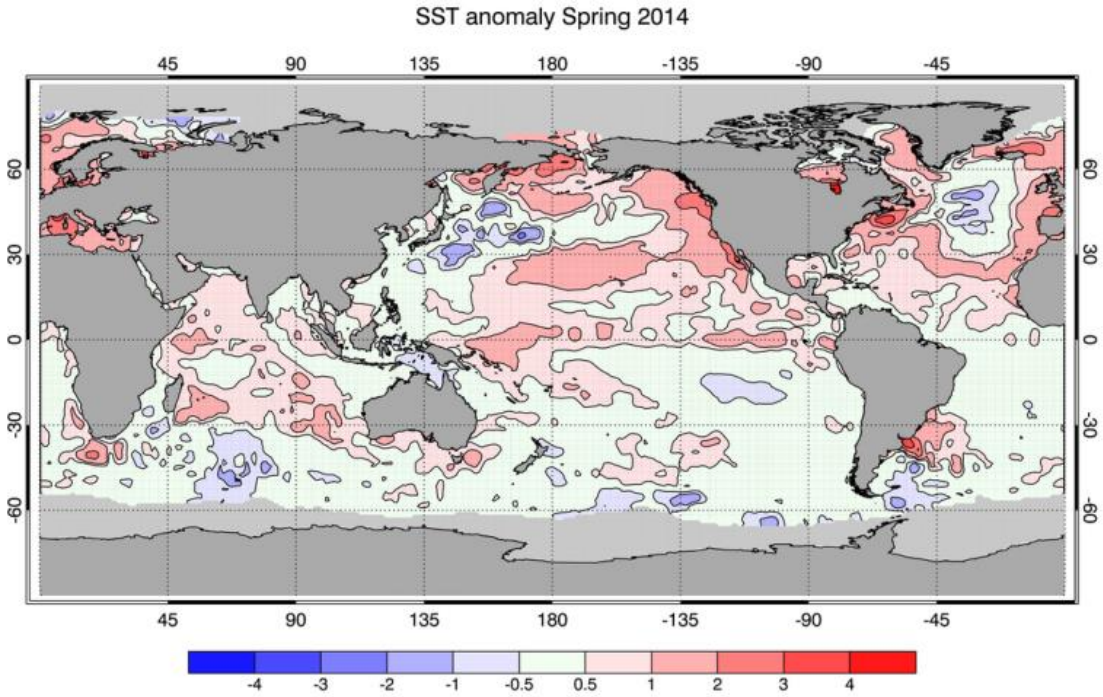

Table 1 NINO SST anomalies for the months of spring 2014, in degrees Celcius, from ftp://ftp.cpc.ncep.noaa.gov/wd52dg/data/indices/sstoi.indices.

Month	NINO1+2 Anomaly	NINO3 Anomaly	NINO4 Anomaly	NINO3.4 Anomaly
September	+0.96	+0.45	+0.65	+0.45
October	+0.75	+0.66	+0.64	+0.49
November	+0.74	+0.91	+0.88	+0.85

Equatorial Pacific sub-surface patterns

The Hovmöller diagram for the 20 °C isotherm depth and anomaly along the equator for March 2012 to November 2014, obtained from the TAO Project Office, is shown in Figure 8. The 20 °C isotherm depth is generally located close to the equatorial thermocline, which is the region of greatest temperature gradient with depth, and is the boundary between the warm near-surface and cold deep-ocean waters. Therefore, measurements of the 20 °C isotherm make a good proxy for the thermocline depth. Positive anomalies correspond to the 20 °C isotherm being deeper than average. A lowering of the thermocline depth results in less cold water available for upwelling, and therefore a warming of surface temperatures. The converse is also true.

Through spring 2014, two downwelling Kelvin waves appear to have deepened the thermocline in the eastern Pacific. These may have been initiated by the winds at 150°E in mid-July and late September.

Figure 8 Time-longitude section of the monthly anomalous depth of the 20 °C isotherm at the equator (2°S to 2°N) for January 2012 to November 2014. (Plot obtained from the TAO Project Office).

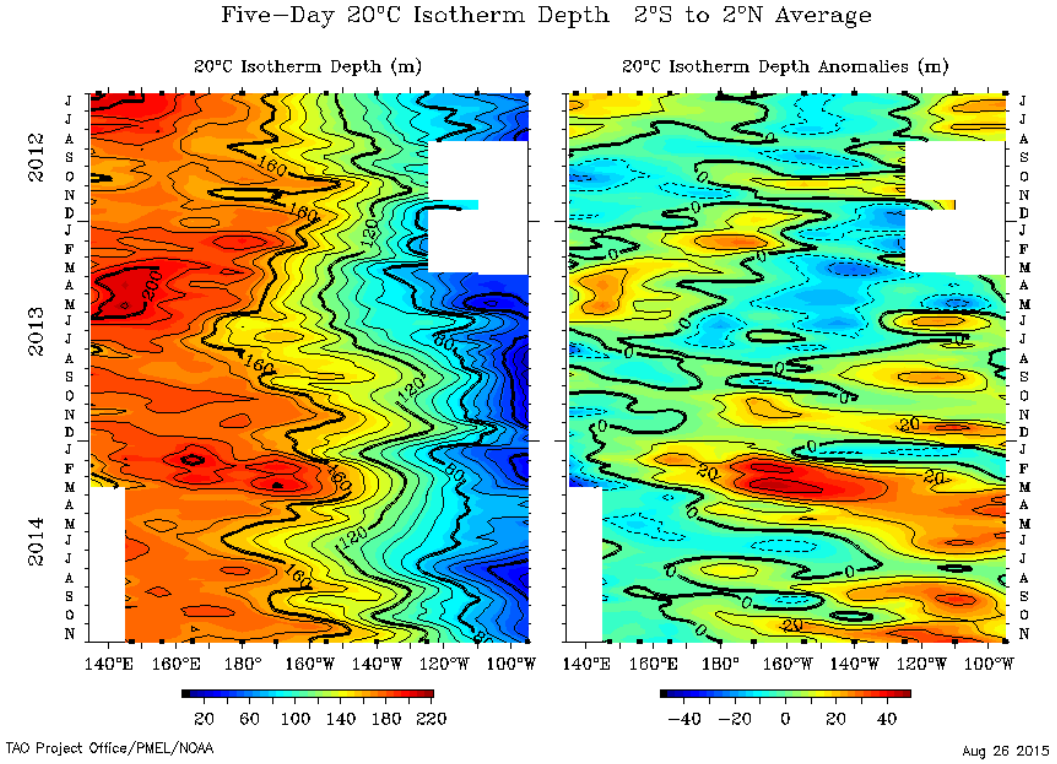

Figure 9 shows a cross-section of monthly equatorial subsurface temperature anomalies across the Pacific from August to November 2014 (obtained from Bureau of Meteorology). Red shading indicates warm anomalies, and blue shading indicates cool anomalies. Through spring, warm anomalies remained at about 170°E, and also started to build right across the basin, until in November surface conditions were anomalously warm across the whole equatorial Pacific, and this extended to at least 150 m depth east of the Date Line. The cool sub-surface anomalies in the far east weakened somewhat, possibly linked to the deepening thermocline evident in Figure 8. In the subsurface in the west, cool anomalies became more established by November.

Figure 9 Four-month sequence from August 2014 to November 2014 of vertical sea subsurface temperature anomalies at the equator for the Pacific Ocean. The contour interval is 0.5 °C. (Plot obtained from http://www.bom.gov.au/oceanography/oceantemp/pastanal.shtml).

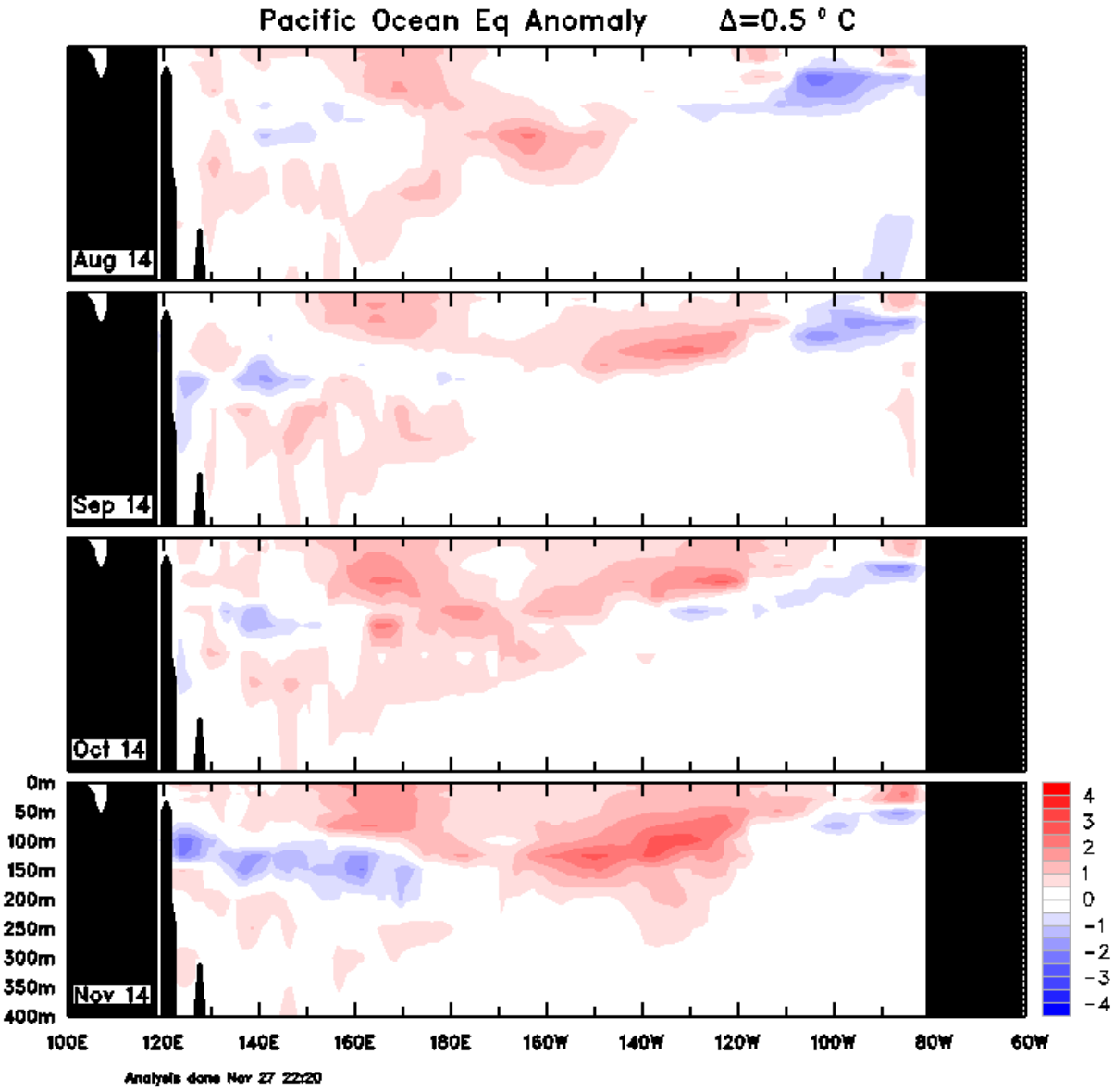

Atmospheric patterns

Surface analysis

The MSLP pattern for spring 2014, computed by the Bureau of Meteorology's Australian Community Climate and Earth-System Simulator (ACCESS) model, is shown in Figure 10, and the associated anomaly pattern in Figure 11. These anomalies are the difference from a 1979–2000 climatology obtained from the National Centers for Environmental Prediction (NCEP) II Reanalysis data (Kanamitsu et al. 2002). The MSLP analysis has been computed using data from the 0000 UTC daily analyses of the ACCESS model. The MSLP anomaly field is not shown over areas of elevated topography (grey shading).

The climatological high pressure centre in the north-eastern Pacific is not evident in the spring average shown in Figure 10, as evidenced by a strong negative anomaly in Figure 11, while the high in the south-east Pacific was enhanced in this season. The climatological high in the north Atlantic is shifted to the west, resulting in a dipole of anomalies, but, as in the Pacific, the climatological high in the south Atlantic was more intense than usual. Pressure was anomalously high over Australia and the Maritime Continent during spring 2014, contributing to the low SOI values mentioned above. To the south-east and south-west of Australia, two low pressure centres are evident. These were likely associated with the record sea ice extent in the Ross Sea and Indian Ocean sector (see Sea Ice section below). They also were part of the atmospheric set-up that contributed to the record warm conditions over Australia through spring.

Figure 10 Spring 2014 MSLP (hPa), 5 hPa contour intervals.

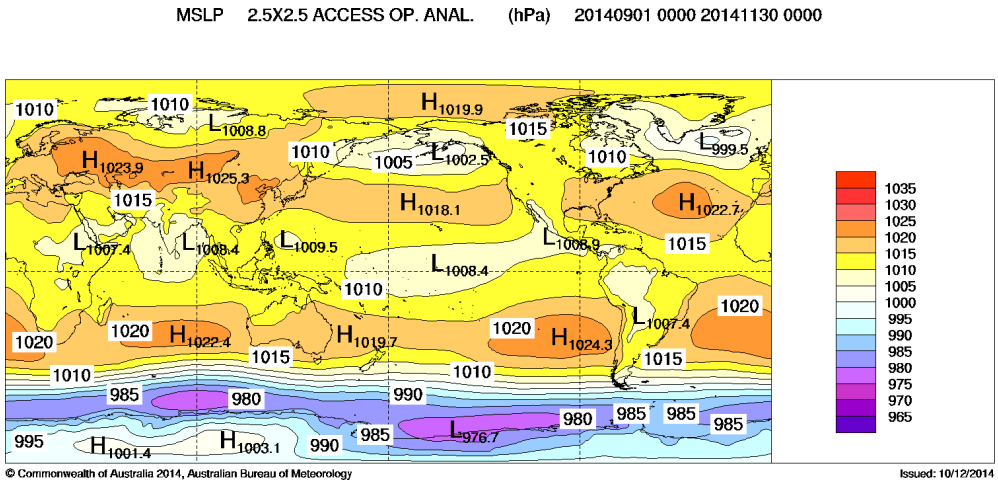

Figure 11 Spring 2014 MSLP anomalies (hPa), from a 1979–2000 climatology.

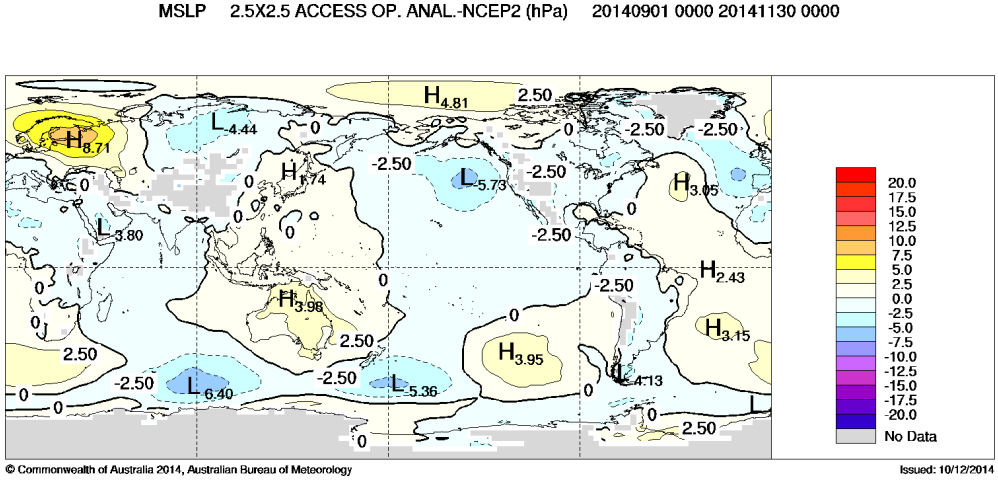

Mid-tropospheric analyses

The 500 hPa geopotential height anomalies (an indicator of the steering of surface synoptic systems across the southern hemisphere, measured in gpm) are shown in Figure 12 for spring 2014, and the 200 hPa geopotential height anomalies are shown in Figure 13. The anomaly pattern for the 500 hPa and 200 hPa geopotential height shows alignment with the MSLP anomaly pattern in the subtropics and high latitudes, with the anomalies becoming more pronounced with height. The persistent high over south east Australia was found to be important for the record heat in the region in October and November (Hope et al. 2015).

Figure 12 Spring 2014 500 hPa mean geopotential height anomalies (gpm), calculated against a 22-year climatology (1979–2000).

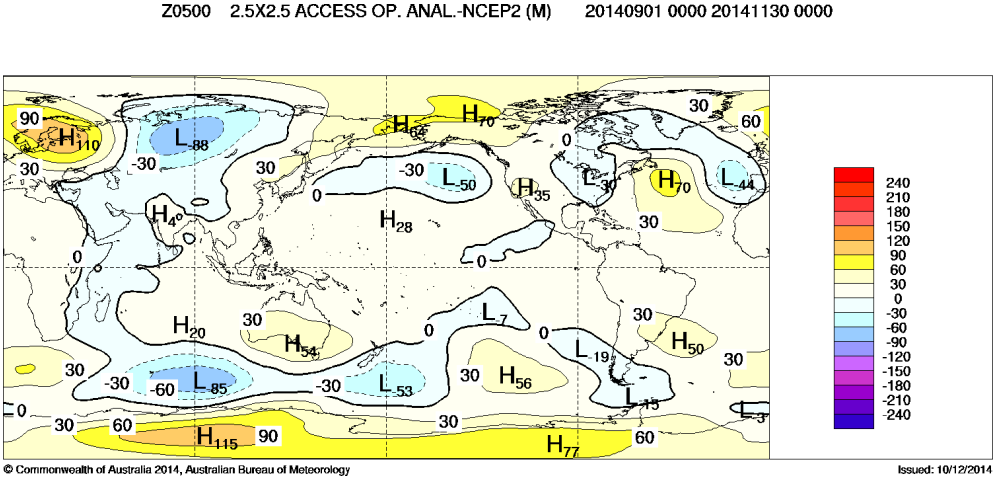

Figure 13 Spring 2014 200 hPa mean geopotential height anomalies (gpm), calculated against a 22-year climatology (1979–2000).

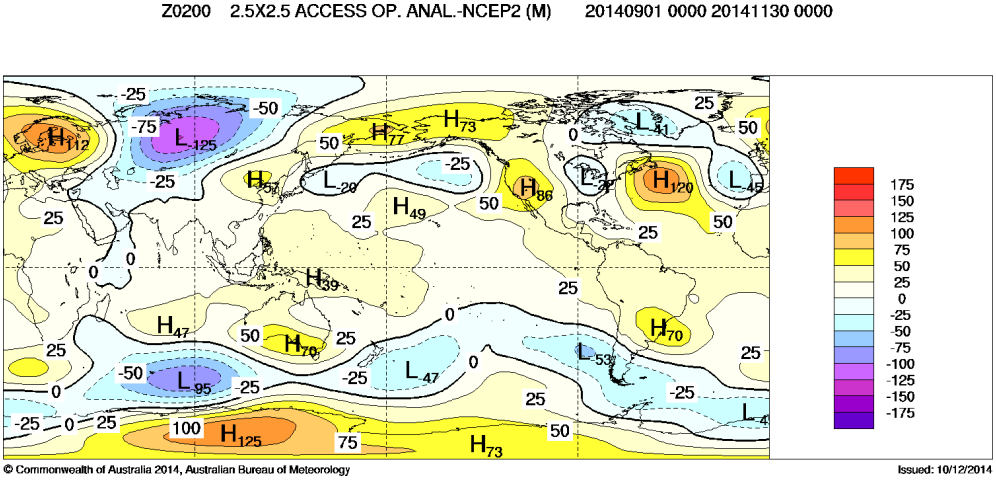

Southern Annular Mode (SAM)

The SAM, also known as the Antarctic Oscillation or AAO, refers to shifts in the location of the belt of strong westerly winds in the middle to high latitudes of the southern hemisphere. Positive phases of SAM are associated with negative MSLP anomalies over Antarctica and positive anomalies in the mid-latitudes. This results in a poleward contraction of the circumpolar belt of westerly winds. Conversely, the circumpolar weserlies are shifted more equatorward when the SAM

index is in its negative phase. In the Australian region negative SAM is associated with westerly wind anomalies, with decreased rainfall and warmer maximum temperatures across eastern Australia during the spring months (Hendon et al., 2007). The MSLP anomaly pattern shown in Figure 11 indicates that the structure of mean MSLP was more 'wavy' than zonal through spring, and projected only weakly onto the SAM index. Aloft (Figure 13), the anomalies were more zonal, and might be said to project onto the negative phase of the SAM. Monthly values reflect this and were weakly negative: –1.119, –0.039 and –0.519 for September, October and November respectively. Although relatively weak, this sign of SAM is historically associated with warm conditions and low rainfall across eastern Australia, and may have helped contribute to the warm observed conditions through October and November (see section below).

Figure 14 Spring 2014 850 hPa vector wind (m s–1), with wind speeds greater than 5 ms-1 shaded.

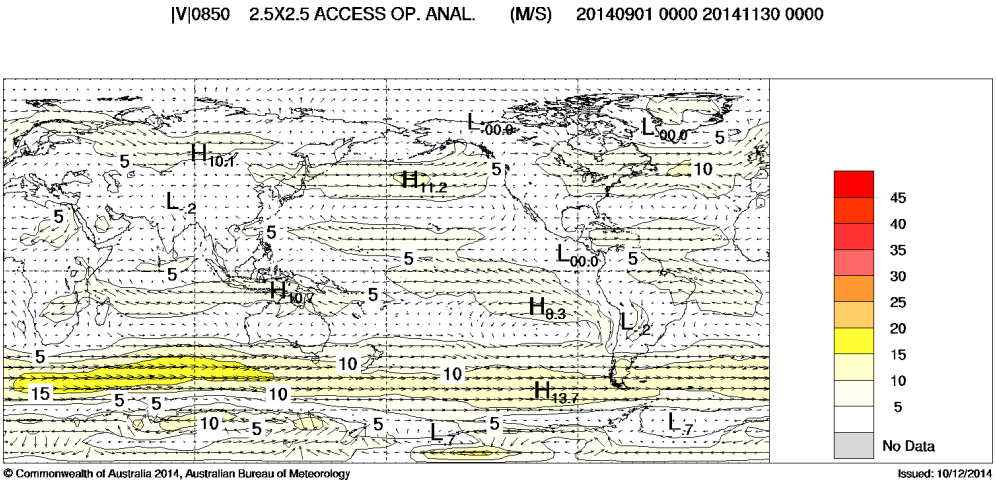

Figure 15 Spring 2014 850 hPa vector wind anomalies (m s–1), calculated against a 22-year climatology (1979–2000). The anomaly field is not shown over areas of elevated topography.

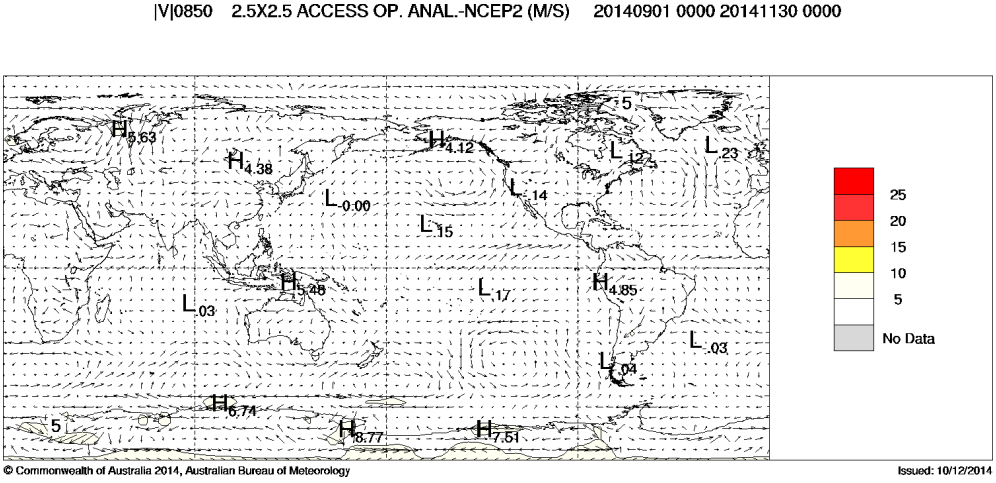

Winds

Mean Spring 2014 low-level (850 hPa) winds are shown in Figure 14, with anomalies shown in Figure 15 (anomalies are from the 22-year NCEP II climatology). Isotach contours are at 5 ms^{-1} intervals. Wind speeds greater than 5 ms^{-1} are shaded in Figure 14. The near-surface wind anomalies (Figure 15) follow as expected from the MSLP anomalies in Figure 11, with an anomalous cyclonic circulation in the north-west Pacific, due to the weakened anticyclone there, while in the south-east Pacific, wind anomalies follow the enhanced anticyclone there. There were also westerly wind anomalies just north of the equator in the central Pacific. The mean winds are still easterly right across the tropical Pacific (Figure 14). The shifted high in the north Atlantic led to anomalous northerly winds. Wind anomalies over Australia were generally from the north, associated with the warm conditions through the season. Around Antarctica winds were strong, but the

anomalies highlight the centres of lows positioned in southern Indian Ocean and south of New Zealand and the strong high in the south Pacific.

Antarctic Sea Ice and Stratospheric Ozone

Sea Ice

September 2014 saw net Antarctic sea-ice extent once again reach record levels (Figure 16; 20.14 million km^2 on 20 September), following successive record sea-ice extent maxima in September 2012 (Reid et al., 2013 and Massom et al., 2013) and 2013 (Massom et al., 2014), see Figure 17. Spring of 2014 was the first time since satellite records began (1979) that sea-ice extent reached over 20 million km^2, and that lasted six consecutive days. Monthly-averaged September sea-ice extent has increased substantially over the last 35 years (Figure 17).

Figure 16 Southern Hemisphere sea ice extent anomaly (percent) with mean MSLP contours (ACCESS-G) for September 2014. Anomalies are calculated with respect to the 1981–2010 climatology.

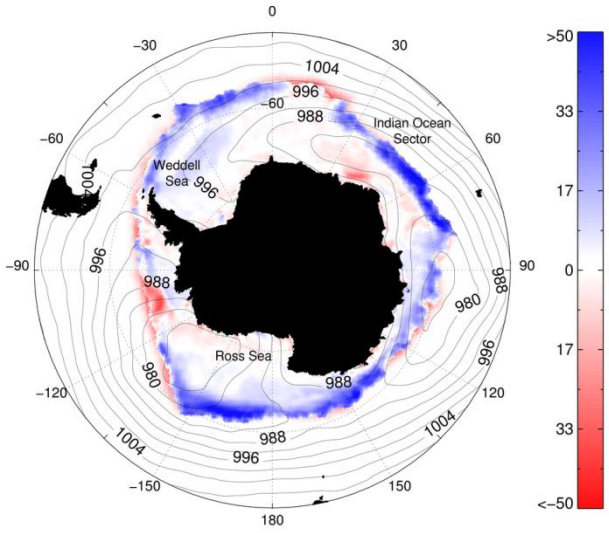

Figure 17 Net Southern Hemisphere sea ice extent anomaly (km^2 x 10^6) for each September from 1979 through 2014, along with the five-year weighted average. Anomalies are calculated with respect to the 1981–2010 climatology.

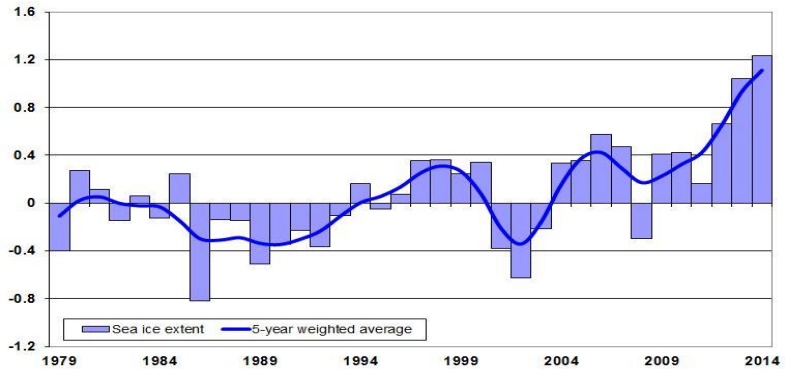

The sea ice extent was particularly high in the Indian Ocean sector and north of the Ross Sea. The record high extent in September 2014 was the result of a combination of cooler-than-normal sea-surface temperatures (Figure 7) and atmospheric wind anomalies (Figure 15) that encouraged ice expansion through Ekman drift and ice formation at the edge of the ice front (Figure 16), but was also primed by well-above-average extent in the month of August. The study by Massonnet et al. (2015) goes into more detail. In early September a deep low pressure system developed just to the east of the Ross Sea

(Figure 11) enhancing ice advection and growth in the Ross Sea. Strong westerly winds in the Indian Ocean sector (Figure 14 and 15) were responsible for ice advance in that region.

Following September's maximum, sea ice began to retreat rapidly during subsequent spring days to be close to average towards the end of November. Much of this reduction in extent occurred in the eastern Weddell Sea where warmer-than-normal north-westerly winds impacted on the ice edge during October and November.

Antarctic Ozone Hole

Figure 18 shows the Antarctic Ozone Hole area (defined as the area where total ozone is less than 220 Dobson Units) for 2014 compared to previous years, based on measurements from the satellite sensors TOMS, OMI and OMPS. The maximum daily area recorded was 23.9 million km^2 in the first week of October, which was only the 18th largest value recorded since the ozone hole was first observed. The 2014 hole was relatively short-lived and closed in early December following unusually short-lived holes in both 2012 and 2013. Further details can be found in the ozone hole report by the Australian Department of Environment[3].

Monthly average polar stratospheric temperatures (expressed as the 60-90° zonal mean at 50 and 100 hPa from the NCEP II Reanalysis) were generally within 1 K of the 1979-2013 climatological mean in winter and early spring, with a preference for slightly below average values. At 10 hPa, temperatures were consistently below average over the period, being up to approximately 4 K below the climatological mean by August. However in the third week of September and then again in mid-October, the magnitude of the poleward eddy heat flux in the lower stratosphere increased sharply, leading to an increase in temperature, a more disturbed polar vortex and a corresponding decrease in ozone hole area.

Stratospheric temperature changes due to the Antarctic Ozone Hole are very likely to have been the dominant driver of the observed changes in Southern Hemisphere tropospheric circulation in summer over recent decades, including an increase in the Southern Annular Mode index, an increase in pressure at mid-latitudes, and a poleward shift of the mid-latitude jet (Arblaster et al. 2014).

Figure 18 Ozone hole area based on OMI & OMPS satellite data. The 2014 hole based on OMI data is indicated by the thick black line while the light blue line indicates the 2014 hole based on OMPS data. The holes for the years 2009 to 2013 are indicated by the thin orange, blue, red, green and pink lines respectively; the grey shaded area shows the 1979 to 2013 TOMS/OMI range and the white line the 1979-2014 mean. Note, the lower bound of the grey area includes days in the early part of the record with no evidence of an ozone hole.

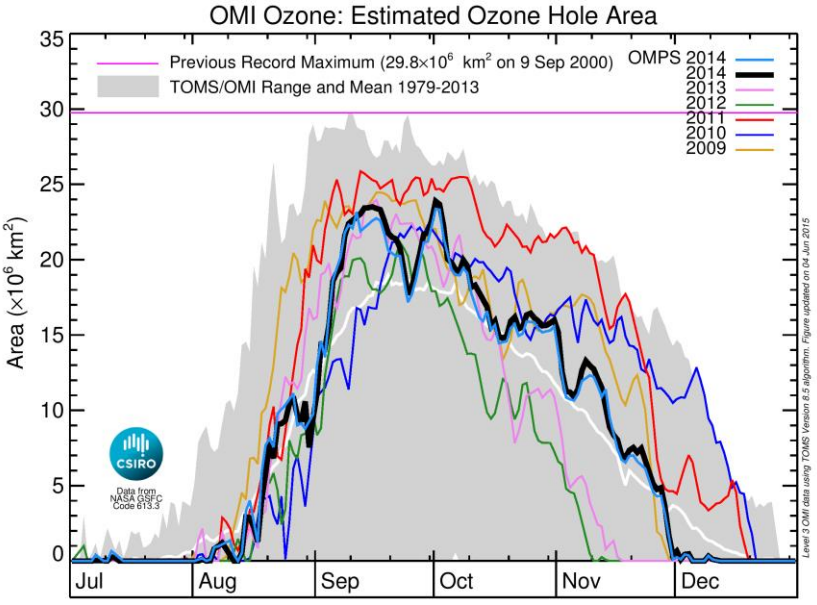

[3] http://www.environment.gov.au/system/files/resources/bde22641-eeb6-4502-9c54-8239c2c64c0f/files/ozone-reports-21-sep-2015.pdf

Australian region

Rainfall

Australian spring rainfall totals for 2014 are shown in Figure 19, while Figure 20 shows the rainfall deciles for the same period. The deciles are calculated with respect to gridded rainfall data for all springs between 1900 and 2014. Spring rainfall averaged over Australia was 49.49 mm, about 32% or 23.0 mm drier than the 1961–1990 average of 72.5 mm (see Table 2). Although late August had some major rainfall events[4] spring was quite dry in the east of the country. Spring rainfall was high across most of Western Australia, with 24.7% in decile 10 (Table 3), and the highest on record in parts of central and southern Western Australia, but lower than average along the western coast of the south-west. Rainfall in spring in the southern half of Western Australia fell in three main events in September and October as well as persistent rainfall in November. Firstly there were two strong cold fronts that crossed the southwest during September, bringing moderate rainfall totals on the 7th and 21st. The former produced severe wind gusts and high tides. A possible tornado was reported on 8 September southeast of Perth in Forrestfield and an apartment block southwest of Perth in Attadale lost its roof. October had one major widespread event just after mid-month when a broad low pressure trough over the interior and a middle level disturbance produced severe thunderstorms and heavy rain (including some daily records for October). Some parts of the interior recorded more than twice their monthly average rainfall for October with 19% of Western Australia recording rainfall totals in the highest 10% of records for October. November was more placid, with rain falling over longer periods in the second and last weeks, but only adding up to decile 10 November rainfall for areas along the southern coast and in the Gascoyne, Pilbara and western Interior.

Figure 19 Spring 2014 rainfall totals (mm) for Australia.

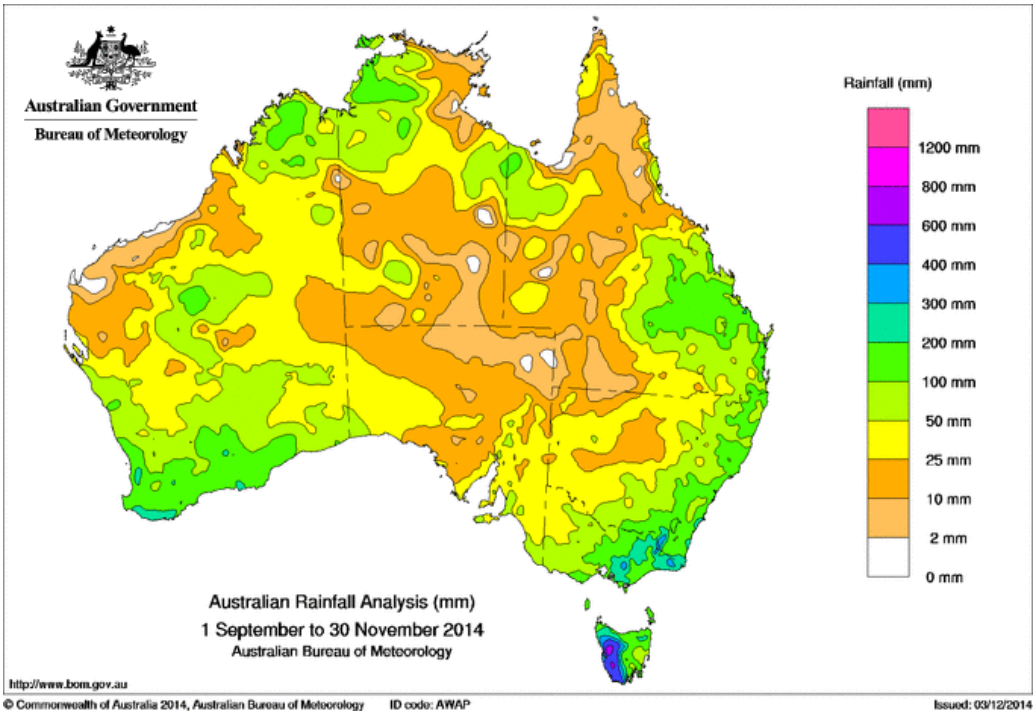

Figure 20 Spring 2014 rainfall deciles for Australia. Decile ranges are based on grid-point values over the springs 1900–2014.

[4] http://www.bom.gov.au/climate/current/month/aus/archive/201408.summary.shtml

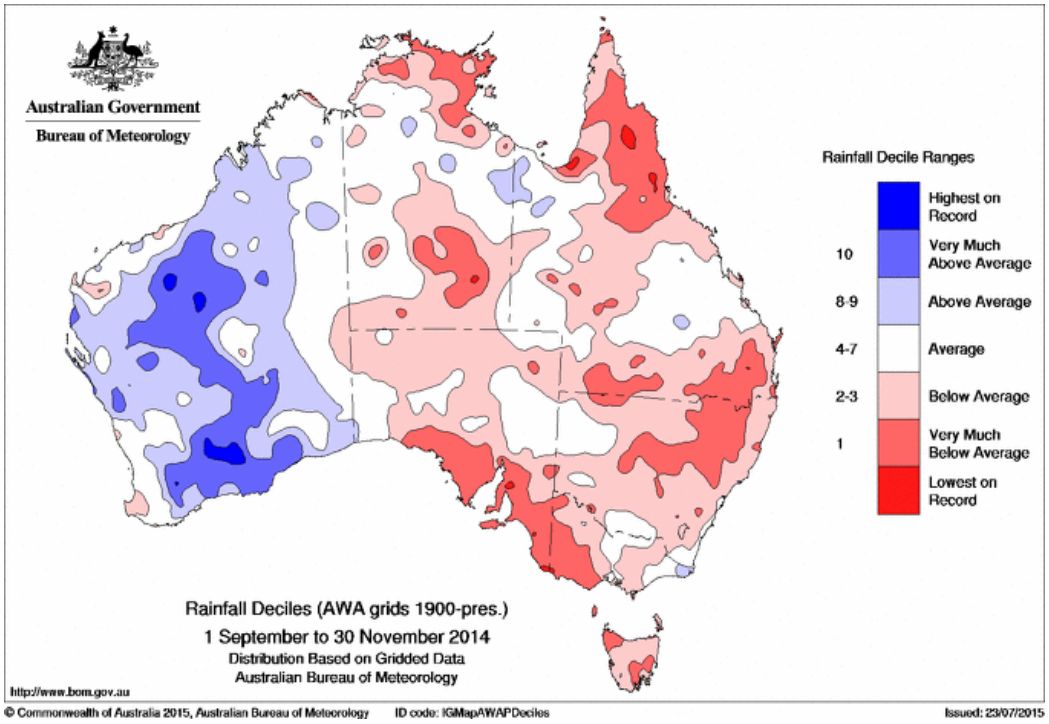

Drought

Spring rainfall in the lowest 10% of historical records across a large part of the south-east of Australia (Table 3) contributed to rainfall deficiencies at longer timescales. Rainfall was below average across large parts of eastern Australia for most of 2014; rainfall deficiencies across parts of the east were exacerbated by particularly dry conditions during October and November. The effect of these rainfall deficiencies was also compounded by record warmth for spring (see following section).

Areas of serious deficiency (below the 10th percentile) persisted in northern New South Wales and southern Queensland (Figure 21). The dry spring conditions also contributed to longer term deficiencies through western Victoria and south-east South Australia (Figure 22). The wet conditions across Western Australia alleviated some of the rainfall deficiencies across the state, though rainfall on the west coast of south-west Western Australia was not above average.

Deficiencies in Queensland were largely a result of poor wet-season rainfall (the northern Australian wet season spans October to April) in the previous two years. Below-average spring rainfall led into another drier-than-average wet season during 2014–15.

As well as short-term rainfall deficiencies (for example, those shown in Figure 21), multi-year deficiencies were evident across parts of eastern Australia (Figure 22) and stretch back to the termination of the 2011–12 La Niña (http://www.bom.gov.au/climate/updates/articles/a010-southern-rainfall-decline.shtml).

Table 2 Summary of the seasonal rainfall ranks and extremes on a national and State basis for spring 2014. The ranking in the last column goes from 1 (lowest) to 115 (highest) and is calculated over the years 1900 to 2014 inclusive.

Region	*Highest seasonal total (mm)*	*Lowest seasonal total (mm)*	*Highest daily total (mm)*	*Area-averaged rainfall (mm)*	*Rank of area-averaged rainfall*	*% difference from mean*
Australia	1040.4 at Mount Read (Tas.)	Zero at several locations	218.0 at Bermagui South (NSW) on 14/10	49.68	31	–31.5
Queensland	235.2 at Montville 'Craglands'	Zero at several locations	131.8 at Springs on 20/11	41.66	15	–50.6
New South Wales	443.4 at Perisher Valley AWS	2.2 at Wanaaring (Owen Downs)	218.0 at Bermagui South on 14/10	61.8	11	–50.2
Victoria	458.2 at Mount Baw Baw	22.7 at Meringur	96.6 at Weeragua (Cann River, East Branch) on 14/10	116.17	15	–35.8
Tasmania	1040.4 at Mount Read	51.4 at Tunbridge (Austin-Vale)	87.8 at Mount Victoria (Una Plain) on 07/10	270.33	12	–26.0
South Australia	121.2 at Piccadilly (Mount Lofty Botanic Garden)	4.6 at Innamincka Station	30.0 at Gluepot Reserve, on 16/11	22.26	13	–56.3
Western Australia	319.8 at Wereroa	Zero at several locations	108.0 at Karrivale on 20/10	56.58	94	+37.9
Northern Territory	250.4 at The Chase	Zero at several locations	109.0 at Northlakes on 28/11	37.95	32	–43.9

Table 3 Percentage areas in different categories for spring 2014 rainfall. ‘Severe deficiency’ denotes rainfall at or below the 5th percentile. Areas in ‘decile 1’ include those in ‘severe deficiency’ which in turn include those which are ‘lowest on record’. Areas in ‘decile 10’ include those which are ‘highest on record’. Percentage areas of highest and lowest on record are given to two decimal places because of the small quantities involved; other percentage areas are given to one decimal place.

Region	*Lowest on record (%)*	*Severe deficiency (%)*	*Decile 1 (%)*	*Decile 10 (%)*	*Highest on record (%)*
Australia	0.54	7.6	15.0	8.1	0.60
Queensland	1.61	12.8	24.2	0.0	0.00
New South Wales	0.17	9.3	25.9	0.0	0.00
Victoria	0.53	20.3	32.8	0.0	0.00
Tasmania	0.00	10.9	35.2	0.0	0.00
South Australia	0.58	14.1	20.0	0.0	0.00
Western Australia	0.00	0.0	0.2	24.7	1.84
Northern Territory	0.38	6.7	16.4	0.0	0.00

Figure 21 Rainfall deficiencies for the 12-month period 1 December 2013 to 30 November 2014. Only those areas in or below the tenth percentile are shown. Percentiles are based on grid-point values over all similar 12-month periods ending November during 1900–2014.

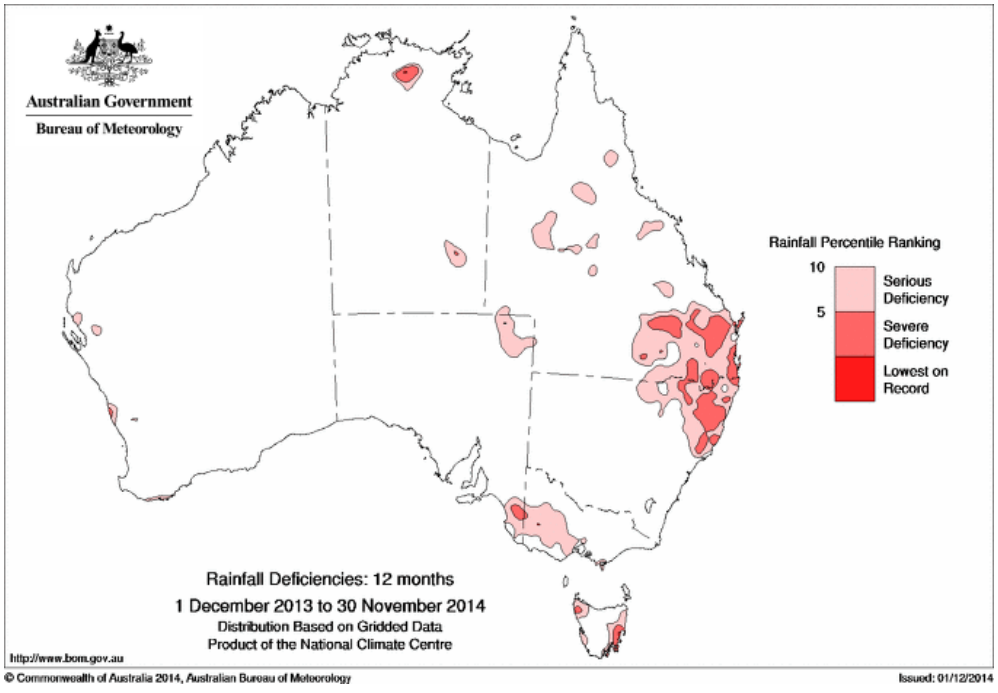

Figure 22 Rainfall deficiencies for the 26-month period 1 October 2012 to 30 November 2014. Only those areas in or below the tenth percentile are shown. Percentiles are based on grid-point values over all similar 26-month periods ending November during 1900–2014.

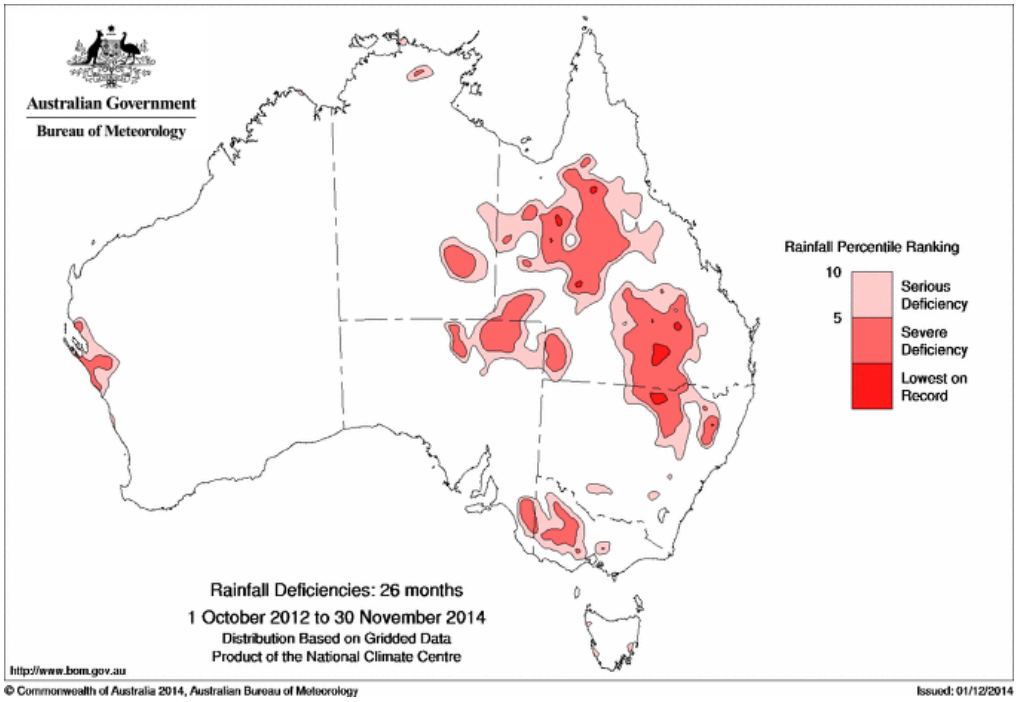

Temperature

Figures 23 and 25 show the maximum and minimum mean daily temperature anomalies (relative to a reference period of 1961–1990), respectively, for spring 2014[5]. Figures 24 and 26 show the corresponding maximum and minimum temperature deciles, calculated using monthly temperature analyses from 1911 to 2014. A summary of percentage areas that had the lowest and highest maximum or minimum temperatures on record for each State and Territory is shown in Table 4, with the lowest and highest decile shown for minimum temperature, but only deciles 9 and 10 for maximum temperature as temperatures were so warm through the season that there were no areas greater than 10 % of a state in any other decile. Decile ranks and extremes by state are shown in Tables 5 and 6 for maximum and minimum temperature respectively. Area-averaged anomalies have been calculated using the Bureau's Australian Climate Observations Reference Network – Surface Air Temperature (ACORN-SAT) dataset[6], while the maps are based on the Australian Water Availability Project (AWAP, Jones et al. 2009) dataset.

Spring 2014 was Australia's warmest on record for both mean and maximum temperatures. Not only did the Australian average seasonal maximum temperature anomaly of +2.32 °C above the 1961–1990 mean surpass the record-breaking spring of 2013, which had a maximum temperature anomaly of +2.06 °C, it was the largest positive mean temperature anomaly recorded for any season (+1.67, the previous record was +1.64 °C set during autumn 2005, records start in 1910; see Special Climate Statement (http://www.bom.gov.au/climate/current/statements/scs50.pdf)). The anomalous heat was greatest in the west of the country in September (Australia-wide maximum temperature anomaly of +2.03 °C, fifth-warmest on record) and across the south and up the east as the season progressed. The Australia-wide monthly maximum temperature anomaly was +2.76 °C for October, and +2.18 °C for November—both records for their respective months. As can be seen in Figure 24, there were extensive regions which had their highest spring maximum temperatures on record, with the only regions that weren't in the top decile being in north-east Queensland, small sections of Western Australia and western Tasmania. All states had state-wide average maximum temperature anomalies that were in the top 5 warmest springs, with New South Wales, South Australia and Western Australia having their warmest spring on record. The

[5] See Jones et al. 2009 for more details relating to the spatial analyses of temperature data.
[6] See http://www.bom.gov.au/climate/change/acorn-sat/index.shtml for a full range of documentation

causes of the October and November heat were explored by Hope et al. (2015). They found that the mean wave train pattern evident in the 200 hPa height in Figure 13 is one most commonly associated with heat in south-east Australia, and in 2014 the ongoing warming of the ocean over the last 50 years contributed to the extreme heat. The negative OLR anomalies in the equatorial Indian Ocean align with the hypothesis that the wave train was promoted by enhanced convection in that region.

Minimum temperatures averaged over spring were slightly less emphatic, being the equal-fifth warmest on record (Table 6). Only Western Australia had a state-wide average approaching the record, ranking as the second-warmest on record, although about two thirds of South Australia and Western Australia had minimum temperatures in the top decile (Figure 26). Some regions were still cool, particularly across the north. National monthly minimum temperature anomalies were: +0.41 °C in September, +1.06 °C in October and +1.74 °C in November (warmest on record for November).

Figure 23 Spring 2014 mean daily maximum temperature anomalies (°C), calculated against a 30-year climatology (1961–1990).

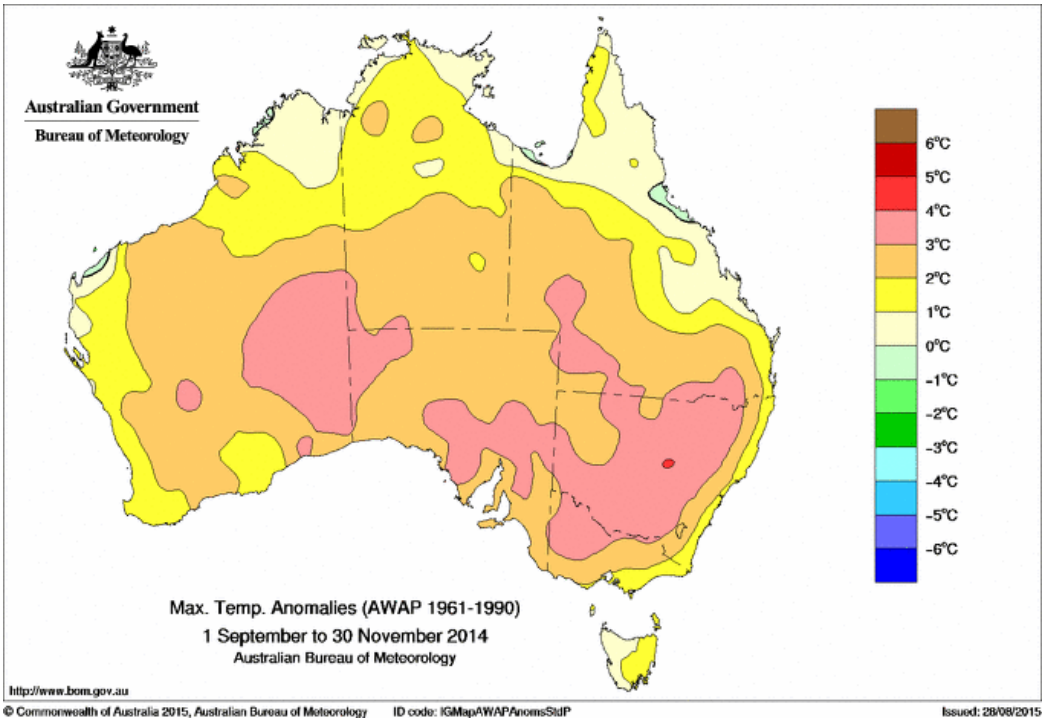

Figure 24 Spring 2014 mean daily maximum temperature deciles. Decile ranges are based on grid-point values over the springs 1910–2014.

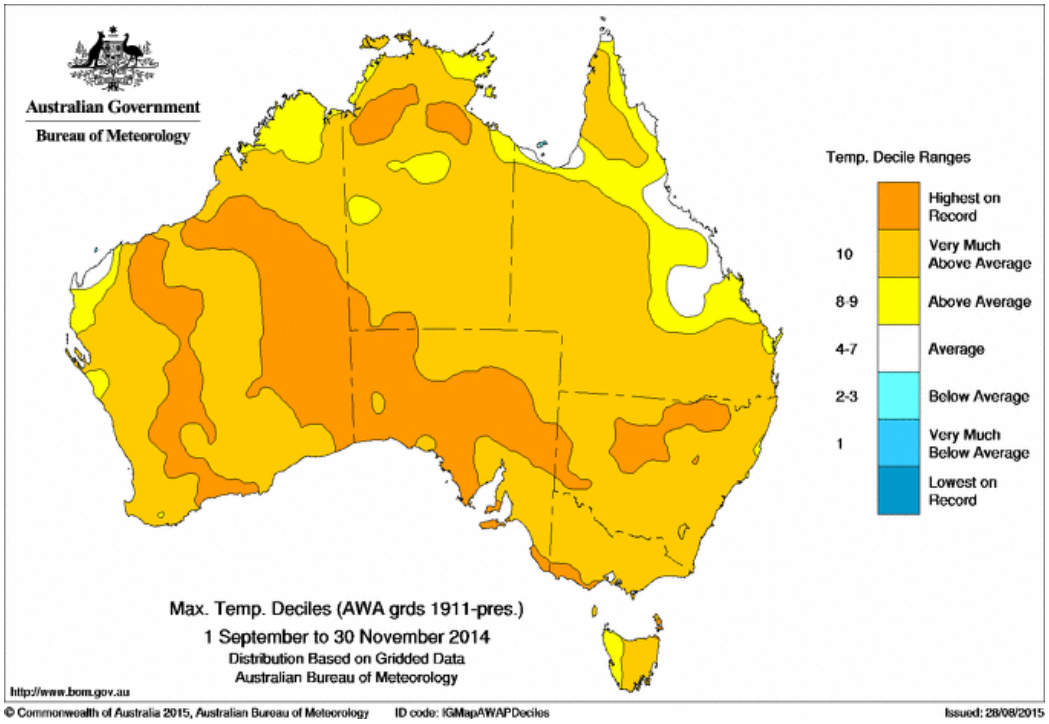

Figure 25 Spring 2014 mean daily minimum temperature anomalies (°C), calculated against a 30-year climatology (1961–1990).

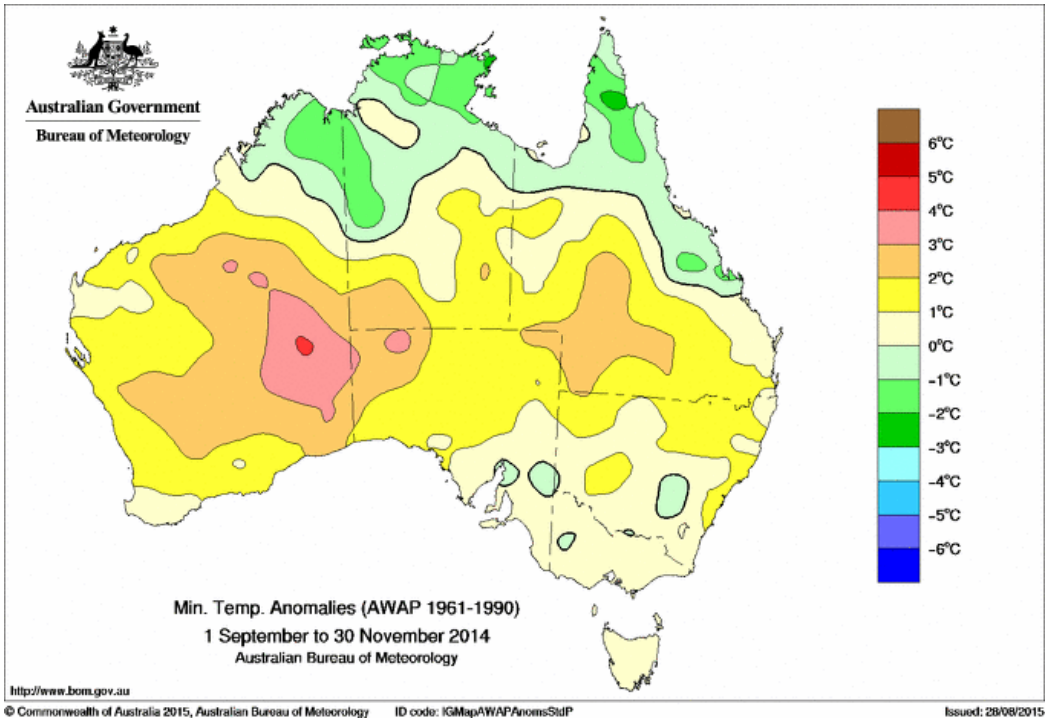

Figure 26 Spring 2014 mean daily minimum temperature deciles. Decile ranges are based on grid-point values over the springs 1910–2014.

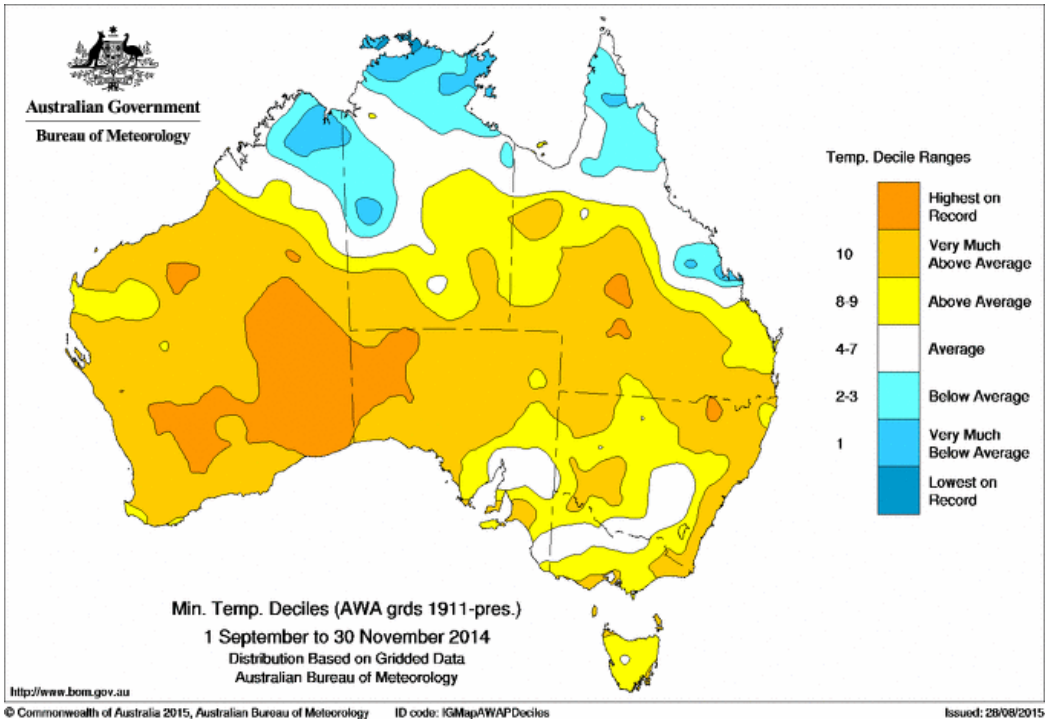

Table 4 Percentage areas in different categories for spring 2014. Areas in "decile 1" include those which are "lowest on record". Areas in "decile 10" include those which are "highest on record". For Maximum Temperatures, there were no areas larger than 10% made up by any decile lower than decile 9. Grid-point deciles calculated with respect to 1910–2014. Area-averaged values are derived from the Australian Bureau of Meteorology AWAP grids (Jones et al., 2009).

	Maximum Temperature				*Minimum Temperature*			
Region	Lowest on record	Decile 9	Decile 10	Highest on record	Lowest on records	Decile 1	Decile 10	Highest on record
Australia	0.00	5.6	89.1	24.6	0.08	2.6	54.3	10.72
Queensland	0.00	10.9	70.7	0.00	0.00	1.3	45.3	1.83
New South Wales	0.00	0.4	99.6	20.5	0.00	0.0	44.4	1.32
Victoria	0.00	0.0	100.0	6.4	0.00	0.0	17.2	0.00
Tasmania	0.00	30.7	69.3	0.00	0.00	0.0	8.1	0.00
South Australia	0.00	0.0	100.0	59.2	0.00	0.0	76.7	13.98
Western Australia	0.00	4.8	92.7	38.3	0.00	2.5	79.2	25.55
Northern Territory	0.00	7.2	90.8	11.9	0.46	8.4	16.8	0.00

Table 5 Summary of the seasonal mean daily maximum temperature ranks and extremes on a national and State basis for spring 2014. The ranking in the last column goes from 1 (lowest) to 105 (highest) and is calculated over the years 1910–2014.

Region	*Highest seasonal mean maximum (°C)*	*Lowest seasonal mean maximum (°C)*	*Highest daily temperature (°C)*	*Lowest daily maximum temperature (°C)*	*Area-averaged temperature anomaly (°C)*	*Rank of area-averaged temperature anomaly*
Australia	40.1 at Fitzroy Crossing (WA)	8.3 at Mount Read (Tas.)	46.1 at Roxby Downs (SA) on 22/11	–2.7 at Thredbo AWS (NSW) on 03/09	2.32	105 Equal-warmest on record (previous 2.06 in 2013)
Queensland	38.2 at Century Mine	24.4 at Cape Moreton	45.3 at Birdsville on 22/11	13.2 at Applethorpe on 03/09	1.88	102
New South Wales	32.6 at Mungindi Post Office	9.4 at Thredbo AWS	45.8 at Bourke Airport on 14/11 and 23/11	–2.7 at Thredbo AWS on 03/09	3.20	105 Warmest on record (previous 3.04 in 2006)
Victoria	27.2 at Mildura	9.6 at Mount Hotham	40.6 at Walpeup on 30/11	–2.5 at Mount Hotham on 02/09	2.63	104 Equal-second warmest on record
Tasmania	19.2 at Friendly Beaches	8.3 at Mount Read	32.1 at Flinders Island Airport on 08/11	–0.6 at Mount Wellington on 02/11	1.01	103 Third warmest on record
South Australia	33.0 at Oodnadatta	18.7 at Neptune Island	46.1 at Roxby Downs on 22/11	9.0 at Mount Lofty on 18/09	3.06	105 Warmest on record (previous 2.74 in 2012 and 2006)
Western Australia	40.1 at Fitzroy Crossing	19.4 at Shannon	45.2 at Bidyadanga on 09/10	12.8 at Shannon on 08/09 and Jacup on 18/10	2.26	105 Warmest on record (previous 1.87 in 2006)
Northern Territory	39.6 at Bradshaw	29.9 at McCluer Island	44.9 at Alice Springs on 13/11	18.2 at Kulgera on 05/09	1.92	104 Second warmest on record

Table 6 Summary of the seasonal minimum temperature ranks and extremes on a national and State basis for spring 2014. The ranking in the last column goes from 1 (lowest) to 105 (highest) and is calculated over the years 1910–2014

Region	*Highest seasonal mean minimum (°C)*	*Lowest seasonal mean minimum (°C)*	*Highest daily minimum temperature (°C)*	*Lowest daily temperature (°C)*	*Area-averaged temperature anomaly (°C)*	*Rank of area-averaged temperature anomaly*
Australia	24.5 at Horn Island (Qld.)	0.8 at Mount Wellington (Tas.)	32.1 at Birdsville (Qld) on 14/11	–8.3 at Thredbo AWS (NSW) on 03/09	1.02	100.5 (Equal-fifth warmest value)
Queensland	24.5 at Horn Island	9.9 at Applethorpe	32.1 at Birdsville on 14/11	–3.0 at Oakey on 04/09	0.84	95
New South Wales	17.0 at Cape Byron	1.3 at Perisher Valley	30.8 at Tibooburra Post Office on 23/11	–8.3 at Thredbo AWS on 03/09	1.22	99
Victoria	12.0 at Gabo Island	2.0 at Mount Hotham	22.8 at Mildura on 14/11	–6.8 at Mount Hotham Airport on 19/09	0.43	87
Tasmania	10.9 at Swan Island	0.8 at Mount Wellington	17.5 at King Island Airport on 8/11	–8.1 at Liawenee on 15/09	0.33	88
South Australia	16.5 at Moomba	6.8 at Keith (Munkora)	32.8 at Moomba on 23/11	–2.3 at Naracoorte on 19/09	1.35	100
Western Australia	26.1 at Troughton Island	7.4 at Wandering	31.5 at Argyle Aerodrome on 24/11	–3.0 at Eyre on 14/10	1.38	104 Second warmest on record
Northern Territory	25.7 at Darwin NTC AWS	14.6 at Alice Springs	31.0 at Tennant Creek on 20/11	0.3 at Arltunga on 03/09	0.33	73

Ozone

Figure 27 shows total ozone measured by the Bureau at its four Dobson spectrophotomer sites, Darwin, Brisbane, Melbourne and Macquarie Island, averaging daily observations from September to November. (All observations types and wavelengths have been included in this Figure). For seasonal means, the interannual variability is determined primarily by

the broad-scale circulation patterns discussed earlier, such as ENSO and SAM, but in particular by the stratospheric Quasi Biennial Oscillation (QBO) (Tully et al. 2013). Correlations are evident between the four locations despite their geographical separation. At all four sites, spring mean ozone was above the 1990-2013 average in 2014 after being below average in 2013, largely attributable to the QBO (expressed as the 50 hPa equatorial wind anomaly) changing sign from positive to negative in early 2014.

Figure 27 Spring mean (September, October, November) total ozone measured at four Bureau of Meteorology Dobson sites. The dotted line shows the 1990-2013 mean.

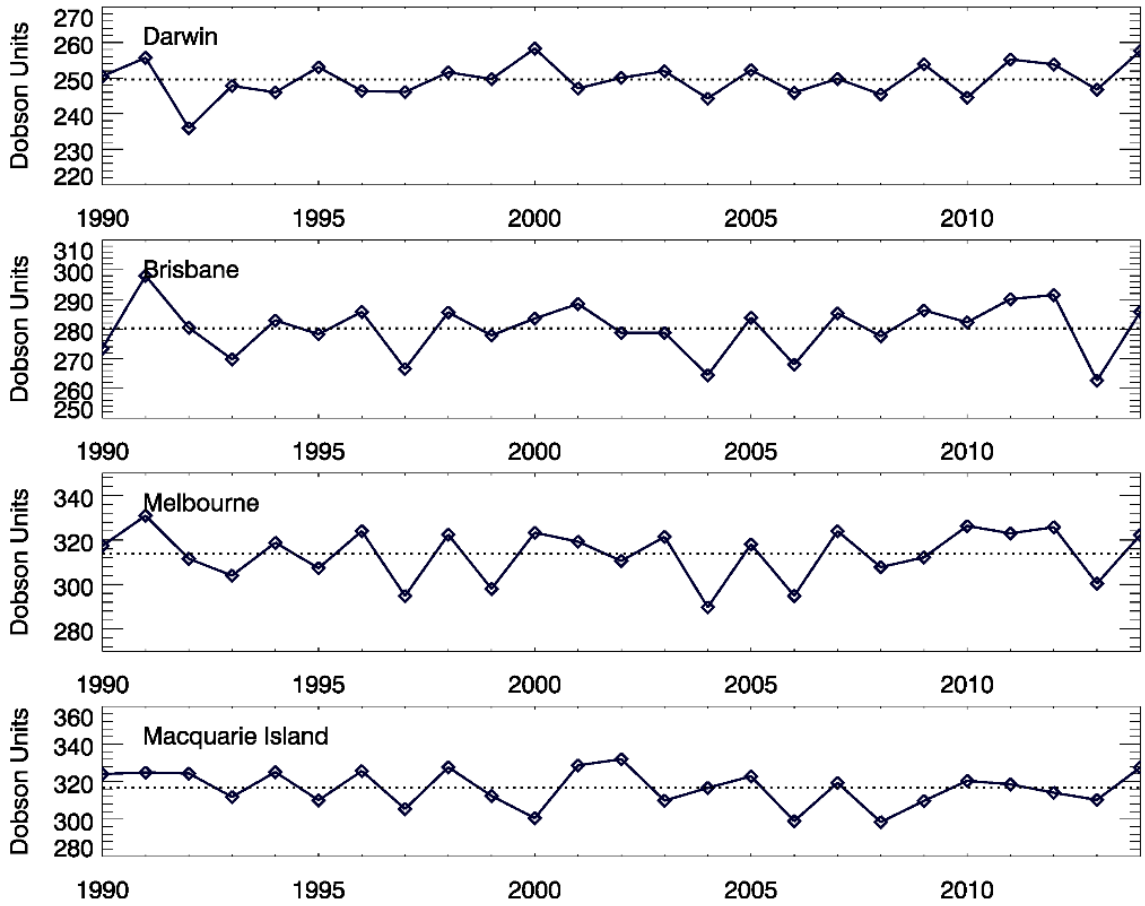

Why did El Niño fail to develop in 2014?

Given the above indicators related to ENSO, why didn't spring 2014 develop into a strong El Nino? A series of westerly wind bursts occurred west of the Date Line between January and April 2014, generating a series of powerful downwelling Kelvin waves that led to anomalous warming in the equatorial cold tongue of the eastern Pacific. Such conditions prime the ocean for an El Niño to occur (e.g. Ganter, 2014). These oceanic conditions may have contributed to 2014 being the warmest year to date on record (Deng, 2015), but as El Niño did not develop, 2014 stands apart from the three previous warmest years as being a year without an El Niño, although it is a year very close to reaching El Niño status.

A possible contributing factor to the failure of El Nino to develop in 2014 may have been the background mean state of the Pacific Ocean. The slowly varying Interdecadal Pacific Oscillation (IPO) was in its negative (cold) phase during 2014, which is a state with similarities to La Niña, but cold tongue anomalies are meridionally broader, extending further into the subtropics than the pattern of anomalies associated with ENSO. When the IPO is in its cold state, El Niño amplitudes tend to be lower (Parker et al. 2007).

The coupling between the ocean and atmosphere required to develop a full El Niño did not occur, and the atmospheric response to the initial oceanic warming and the positive ocean-atmosphere feedbacks that characterize El Niño evolution did not materialize. As outlined above, there was little subsequent activity in the atmosphere, with no further westerly wind bursts, and the coupling between the ocean and atmosphere did not transpire (e.g. McPhaden, 2015; Menkes et al. 2015; Chen et al., 2015). The process of forecasting the 2014 event, and the fact that some agencies said it would be an El Niño year, along with the media reaction, were discussed by Glantz (2015).

Acknowledgements

The authors would like to thank Matthew Wheeler for producing the RMM MJO plot, Joel Lisonbee for making the Bureau of Meteorology's tropical notes available and Eun-Pa Lim for her discussion about the lack of development of an El Niño in 2014.

References

Arblaster, J.M. and N.P. Gillett (Lead Authors), N. Calvo, P.M. Forster, L.M. Polvani, S.-W. Son, D.W. Waugh, and P.J. Young, 2014, Stratospheric ozone changes and climate, Chapter 4 in *Scientific Assessment of Ozone Depletion: 2014*, Global Ozone Research and Monitoring Project – Report No. 55, World Meteorological Organization, Geneva, Switzerland.

Chen, D., T. Lian, C. Fu, M. A. Cane, Y. Tang, R. Murtugudde, X. Song, Q. Wu, and L. Zhou 2015, Strong influence of westerly wind bursts on El Nino diversity. *Nature Geosci*., 8, 339-345.

Deng, B. 2015, 2014 was the hottest year on record. *Nature*, doi:10.1038/nature.2015.16674.

Ganter, C. 2014, Seasonal climate summary southern hemisphere (autumn 2014): tropical Pacific experiences strong push towards El Niño**.** *Aust. Met. Oceanogr. J*., 64, 345-356.

Glantz, M. 2015, Shades of Chaos: Lessons learned about forecasting El Niño and its impacts. *Int. J. Disaster Risk Sci.*, 6, 94-103.

Hendon, H., D. W. J. Thompson, and M. C. Wheeler, 2007: Australian rainfall and surface temperature variations associated with the Southern Hemisphere Annular Mode. *J. Climate*, 20, 2452-2467.

Hope, P, E-P Lim, G Wang, H H Hendon, and J M Arblaster, 2015, Contributors to the record high temperatures across Australia in late spring 2014. In: Explaining extremes of 2014 from a climate perspective, S. C. Herring, M. P. Hoerling, T. C. Peterson, and P. A. Stott (Eds), *Bull. Amer. Meteor. Soc.*, S149-S153; Supplementary material: doi:10.1175/BAMS-D-15-00096.2

Jones, D. A., W. Wang, and R. Fawcett. 2009. High quality spatial climate data-sets for Australia. *Aust. Met. Oceanogr. J.*, 58, 233–248.

Kanamitsu, M., Ebisuzaki, W., Woollen, J., Yang, S.-K, Hnilo, J.J., Fiorino, M. and Potter, G.L. 2002. NCEP-DOE AMIP-II Reanalysis (R-2). *Bull. Amer. Meteor. Soc.*, 83, 1631-43.

Kuleshov, Y. Qi, L., Fawcett, R., Jones, D. 2009, Improving preparedness to natural hazards: Tropical cyclone prediction for the Southern Hemisphere, In: Gan, J. (Ed.), Advances in Geosciences, Vol. 12 Ocean Science, World Scientific Publishing, Singapore, 127–43.

Massom, R.A., P. Reid, S. Stammerjohn, S. Barreira, J. Lieser and T. Scambos. 2013, Antarctic sea ice extent & concentration. In: Blunden, J., & D. S. Arndt, Editors: State of the Climate in 2012. *Special Supplement to the Bulletin of the American Meteorological Society*, 93, S157-S159.

Massom, R.A., P. Reid, S. Stammerjohn, S. Barreira, T. Scambos, and J. Lieser 2014, [Antarctic] Sea ice extent, concentration, and duration. In: State of the Climate in 2013. *Special Supplement to the Bulletin of the American Meteorological Society*, 95, S150-S152.

Massonnet, F., V. Guemas, N. S. Fučkar, and F. J. Doblas-Reyes 2015, The 2014 high record of Antarctic sea ice extent. In: Explaining extremes of 2014 from a climate perspective, S. C. Herring, M. P. Hoerling, T. C. Peterson, and P. A. Stott (Eds), *Bull. Amer. Meteor. Soc*., S163-S167; Supplementary material: doi:10.1175/BAMS-D-15-00093.2

McPhaden, M., 2015, Who killed the big 2014-15 El Niño? EGU General Assembly Conference Abstracts, 2564.

Menkes, C., M. Lengaigne, J. Vialard, M. Puy, P. Marchesiello, S. Cravatte, and G. Cambon, 2015, Why a strong El Niño did not develop in 2014. *EGU General Assembly Conference Abstracts*, 106.

Parker, D., C. Folland, A. Scaife, J. Knight, A. Colman, P. Baines, and B. Dong, 2007, Decadal to multidecadal variability and the climate change background. *J. Geophy. Res.*, 112, D18115, doi:10.1029/2007JD008411

Reid, P.A., M.B. Tully, A.R. Klekociuk, P.B. Krummel and S.K. Rhodes 2013, Seasonal climate summary Southern Hemisphere (spring 2012): Warmer and dryer across much of Australia, along with a new Southern Hemisphere sea ice extent record. *Austr. Met. Oceanogr. J*. 63, 427-442.

Reynolds, R.W., Rayner, N.A., Smith, T.M., Stokes, D.C. and Wang, W. 2002, An improved in situ and satellite SST analysis for climate. *J. Climate*, 15, 1609-25.

Troup, A.J. 1965. The Southern Oscillation. *Quart. J. Roy. Meteor. Soc*., 91, 490-506.

Tully, M.B., Klekociuk, A.R. & Rhodes, S.K., 2013. Trends and Variability in Total Ozone from a Mid-Latitude Southern Hemisphere Site: The Melbourne Dobson Record 1978–2012. *Atmos.-Ocean*, 53, pp.58–65,doi:10.1080/07055900.2013.869192.

Wheeler, M. C. and H. H. Hendon, 2004, An all-season real-time multivariate MJO index: Development of an index for monitoring and prediction. *Mon. Weather. Rev*., 132, 1917-1932.

Wolter, K. and Timlin, M.S. 1993, Monitoring ENSO in COADS with a seasonally adjusted principal component index. *17th Climate Diagnostics Workshop, Norman, OK*, NOAA/NMC/CAC, NSSL, Oklahoma Clim. Survey, CIMMS and the School of Meteorology, Univ. of Oklahoma, 52-7.

Wolter, K. and Timlin, M.S. 1998, Measuring the strength of ENSO – how does 1997/98 rank? *Weather*, 53, 315-24.